ACS APPLIED MATERIALS & INTERFACES

Research Article

www.acsami.org

Size-Dependent Maximization of Upconversion Efficiency of Citrate-Stabilized β-phase $NaYF_4$:Yb^{3+},Er^{3+} Crystals via Annealing

Nathan C. Dyck,[†] Frank C. J. M. van Veggel,[‡] and George P. Demopoulos*,[†]

[†]Materials Engineering, McGill University, 3610 University Street, Montreal, Quebec, Canada H3A 0C5

[‡]Department of Chemistry, University of Victoria, 3800 Finnerty Road, Victoria, British Columbia, Canada V8W 3V6

Supporting Information

ABSTRACT: Upconversion materials show great potential in converting infrared light to visible for many optoelectronic and photovoltaic devices. One of the most promising upconverting materials is Yb^{3+},Er^{3+}- doped β-$NaYF_4$. In this study, annealing is shown to have a significant impact on the phase, morphology, and upconversion luminescence of β-$NaYF_4$:Yb^{3+},Er^{3+} crystals of varying sizes (300 nm, 700 nm, and 2.3 μm, respectively) prepared by hydrothermal synthesis stabilized with sodium citrate. Upconversion luminescence is maximized via annealing while maintaining crystal shape and size dispersity up to a temperature dependent on initial size, with NIR-to-visible quantum yields of 2−5%. Further temperature increases result in growth and agglomeration, increasing luminescence, followed by transformation to the α-cubic phase resulting in decreases in overall upconversion performance and shifts to dominant red emission. This study establishes the critical link between annealing temperature and maximal upconversion luminescence in β-$NaYF_4$:Yb^{3+},Er^{3+} crystals, while maintaining particle morphology, which can be very important for technological application.

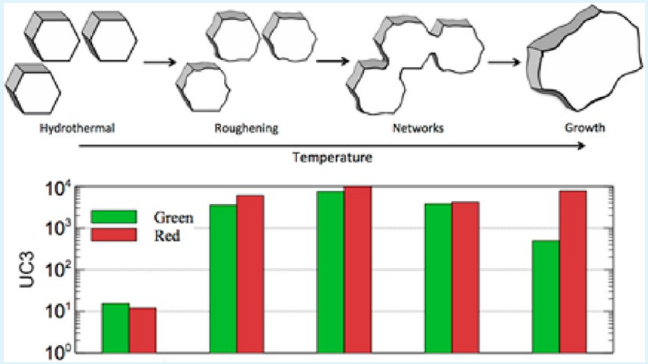

KEYWORDS: *upconversion, annealing, $NaYF_4$:Yb^{3+},Er^{3+}, nanocrystals, microcrystals, hydrothermal, citrate*

1. INTRODUCTION

Upconversion is a process in which two or more low-energy photons are converted to a single high-energy photon. This process is possible in a number of different materials, however lanthanide doped optical host materials are the most common and efficient upconverters available today.[1] While a number of host materials exist, $NaYF_4$ is the most efficient thanks to its low phonon energy, minimizing the nonradiative pathways for upconverted energy states.[2] $NaYF_4$ converts infrared light to green and red when doped with Yb^{3+} and Er^{3+} with the optimal doping concentration 18 at% Yb^{3+} and 2 at% Er^{3+} replacing Y^{3+} in the lattice.[3]

Upconversion from infrared to visible wavelengths has garnered a great deal of attention in recent years due to potential applications in biological markers,[4−7] photonic devices,[8−10] and solar cells.[11−13] Many of these studies employ synthesis methods for producing particles on the order of nanometers to micrometers with many different particle shapes including nanospheres, nanorods, nanotubes, and microplates.[5,7,14−17] In general, smaller upconversion particles on the order of tens to hundreds of nanometers are used in biological applications, while larger particles on the order of hundreds of nanometers to a few micrometers are used in photonic and photovoltaic devices. The overall efficiency of bulk $NaYF_4$:Yb^{3+},Er^{3+} is modest, and when the crystal size is reduced to the micro or nanoscale, the upconversion efficiency also suffers because of a number of different phenomena. Smaller nanoparticles introduce quenching sites including lattice defects that occur due to lower temperatures associated with colloidal synthesis[18] and surface recombination centers due to a drastic increase in surface area.[19] The diffusion length of the intermediate excited Yb^{3+} states has been shown to be on the order of micrometers so when the particle size is smaller than this, it is more difficult for two intermediate states to combine and form an upconverted state before relaxing.[20] In addition, depending on synthesis technique, the doping profile in nanoparticles is not necessarily homogeneous,[21] and it has been shown that surface segregation of the Er^{3+} ions in smaller particles can decrease upconversion due to an increase in cross relaxation that occurs at higher Er^{3+} concentrations.[22] Solution-based synthesis methods also often employ chelating agents such as sodium citrate, oleic acid, or EDTA.[15,18,23,24] It has been suggested that preparation using these ligands can lead to upconversion-quenching defects in the crystal lattice depending on the type of ligand used.[18,23,24] These organic molecules also remain on the surface of the produced crystals, and vibrational states can provide further pathways for nonradiative recombination of the upconverted states.[25]

Received: August 1, 2013
Accepted: October 30, 2013
Published: October 30, 2013

Increasing and maximizing the efficiency of the upconversion process is important to many technological applications. A number of strategies exist for increasing the upconversion in small particles. Core−shell studies have shown to increase the upconversion luminescence.[26,27] In these materials, the shell separates the upconverting core from the surface thereby decreasing the possibility for surface quenching nonradiative pathways and can lead to increases in upconversion up to 7 times in $NaYF_4$:Yb,Er materials.[27] This same effect also helps to increase the green to red ratio, with values as high as 30 in a study by Mai et al.[26] Another study by Wang et al. used time-resolved spectroscopy to investigate the kinetics of the upconversion process and showed that core−shell upconversion materials have a longer luminescent lifetime compared to their core only counterparts, further illustrating the mechanism of enhancement.[25] The same study also pointed out the impact of localized annealing caused by high excitation power (>150 W/cm^2), which can alter the upconversion spectrum. Other studies aim to increase the upconversion luminescence by altering the crystal structure through postsynthesis chemical treatment. Fu et al. showed that the Na^+ content in the crystal lattice is a very important aspect in maximizing upconversion luminescence through ion-insertion via a novel two-step synthesis method.[28] Both core−shell strategies as well as crystal modifications via 2-step synthesis increase the complexity of synthesis and potential material cost.

A much simpler strategy for enhancing upconversion of lanthanide-doped crystals is by controlled annealing. Annealing has been shown to increase the luminescence in upconversion phosphors through crystal refinement,[5] however care must be taken to avoid crystal agglomeration and phase transformation to the α-cubic phase, which is known to have poorer upconversion properties compared with the β-hexagonal phase.[3] Using chelating agents as crystal modifiers like sodium citrate during hydrothermal synthesis allows for stabilization and size control of the β-phase but this comes at the expense of upconversion intensity.[18] Recently, we reported that annealing can significantly increase the upconversion luminescence of surfactant-modified upconversion crystals,[29] however the annealing temperature was not optimized and annealing while maintaining crystal morphology was not studied nor achieved. In this study, the effect of annealing on the phase, morphology and upconversion luminescence in citrate-stabilized, β-$NaYF_4$:Yb^{3+},Er^{3+} phosphors of different sizes is investigated in detail. An effort is made to maximize upconversion while limiting morphological changes, which can be detrimental to technological application of the phosphor powders. Through optimization of the annealing conditions, it is demonstrated that even submicrometer sized nanocrystals (300 nm) can be produced with infrared-to-visible quantum yields that are comparable with bulk crystals.

2. EXPERIMENTAL SECTION

Crystal Synthesis. The synthesis procedure used is based on prior work accomplished in our lab.[29,30] $NaYF_4$:18%Yb^{3+},2%Er^{3+} was produced by a citrate stabilized hydrothermal method. Typically, an amount of sodium citrate (2.3, 11, or 54 mmol) was dissolved into 40 mL of deionized water. Following this, $Y(NO_3)_3{\cdot}6H_2O$ (1.6 mmol), $Yb(NO_3)_3{\cdot}5H_2O$ (0.36 mmol), and $Er(NO_3)_3{\cdot}5H_2O$ (0.04 mmol) was added to the solution and stirred until dissolved. Finally, an amount of NaF (18 mmol) was added to the solution and stirred for 15 min. The solution was transferred to a 125 mL stainless steel pressure vessel (Parr Instruments) with Teflon liner and heated hydrothermally at 200 °C for 2 or 24 h, depending on sample type. The citrate concentration and hydrothermal reaction time were set in order to obtain β-phase particles of specific size according to previous work in our lab.[29,30] A summary of these parameters is found in Table 1. After hydrothermal

Table 1. Hydrothermal Synthesis Parameters for Different Size Upconversion Crystals Studied

sample	$[Ln^{3+}]$ (mmol)	[NaF] (mmol)	$[Cit^{3-}]$ (mmol)	time (hours)	temperature (°C)	SEM crystal size (nm)
UC1	2	18	2.3	24	200	2300
UC2	2	18	11	24	200	700
UC3	2	18	54	2	200	300

treatment, the resulting precipitate was separated by centrifugation and then washed 3 times with deionized water and once with ethanol. The resulting solids were dried at 80 °C for 24 h. Each sample type was split into equal portions and annealed for 2 h in air at temperatures between 400 and 700 °C after which it was air quenched giving final powder samples for analysis.

Undoped reference samples were made using an identical procedure, maintaining the concentration of trivalent salts (2 mmol) without the addition of $Yb(NO_3)_3$ or $Er(NO_3)_3$. The reference samples were subjected to the same annealing conditions as their doped counterparts.

Characterization. Powders were characterized before and after annealing by powder X-ray diffraction (XRD), scanning electron microscopy (SEM), transmission electron microscopy (TEM), ATR-FTIR, TGA, upconversion luminescence, and absolute quantum yield measurements.

XRD analysis was done using a Bruker Discover D8 diffractometer with $\lambda_{Cu,K\alpha}$ = 1.5406 Å radiation operated at 40 kV and 20 mA. A VANTEC 2000 2D X-ray area detector was used with a 2θ frame width of 23° and angular scanning resolution of 0.05°. Four frames were collected for each sample at 50 s/frame. Analysis was done using the Eva software package provided by Bruker. SEM analysis was done using a Hitachi S-4700 FE-SEM. TEM analysis was done using a Philips CM200 TEM operated at 200 kV. ATR-FTIR analysis was done using a Perkin-Elmer Spectrum Two IR spectrometer with ATR accessory. Scans were taken from 4000 to 400 cm^{-1}.

Upconversion spectra were collected from 450 to 700 nm with 0.5 nm step size and 2 nm emission slit using a Fluoromax-2 spectrophotometer with a 980 nm IR laser diode (100 mW, Startech) as excitation source. The power density and spot size were approximately 2.5 W/cm^2 and 0.05 cm^2, respectively. The fluorescence was measured using the solid powder; the laser spot size was kept the same when comparing samples, ensuring that the interaction volume and laser intensity was the same from sample to sample. The measurement spectra of all samples are recorded under the same conditions and were corrected for the spectral response of the spectrometer. The position of the laser relative to the samples was identical during all measurements. Each sample was immobilized and pressed between two glass slides to ensure a flat surface and uniform packing, and fixed using a metallic sample holder. All annealed samples were ground using a mortar and pestle prior to measurement to minimize aggregation. Upconversion luminescence was quantified by integrating the emission peaks from the obtained spectra. For simpler comparison purposes, integrated values were normalized to the highest emitting samples for each particle size type.

Quantum yield measurements were performed using a procedure following Boyer et al.,[31] using a 100 mW NIR laser as excitation, an integrating sphere, a visible spectrometer and photomultiplier tube for measuring the upconverted visible signal, and a NIR spectrometer and photomultiplier tube for measuring the absorbed NIR light. The power density and spot size were approximately 50 W/cm^2 and 0.0023 cm^2, respectively. A neutral density filter (10000×) was used to ensure that the NIR PMT was not saturated. Spectra were taken as an average of 5 individual scans with a monochromator slit size of 0.5 nm and were corrected for the spectral response of the corresponding spectrometer.

The relative sensitivity of the visible and NIR spectrometers was calibrated using a tungsten lamp. A schematic of the experimental setup is shown in Figure 1. The laser light was incident on the solid

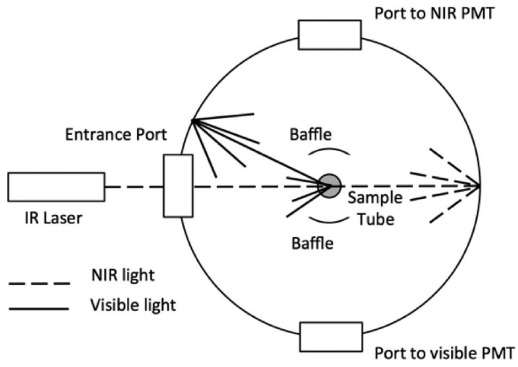

Figure 1. Experimental setup schematic for measuring quantum yield of upconversion crystals.

powder sample immobilized in a modified EPR tube. A micrometer was used to ensure consistent positioning of the EPR tubes. Baffles were employed to ensure no upconverted or scattered light was incident on the detectors without first interacting with the integrating sphere. In order to accurately determine the absorption of the doped sample, an undoped reference sample was used as a baseline, duplicating the scattering effect of the sample powder and ensuring the difference between reference and sample was only due to absorption.

3. RESULTS AND DISCUSSION

Each crystal sample produced was in the form of a white powder. In the case of sample types treated hydrothermally for 24 h (UC1 and UC2), the hydrothermal supernatant solution was brown in color indicating decomposition of residual citrate molecules in solution.

Upconversion luminescence was measured in all samples (a sample emission spectrum can be found in Supporting Information, Figure S1). $NaYF_4$:Yb^{3+},Er^{3+} emits visible light in two regions: green (510 nm −560 nm, corresponding to the $^2H_{11/2} \rightarrow {}^4I_{15/2}$ and $^4S_{3/2} \rightarrow {}^4I_{15/2}$ transitions in Er^{3+}) and red (640 nm −670 nm, corresponding to the $^4F_{9/2} \rightarrow {}^4I_{15/2}$ transition in Er^{3+}). In order to easily compare upconversion between samples, the area under the peaks was integrated, resulting in a single value. For green emission, peaks were integrated from 500 to 575 nm, and for red emission, peaks were integrated from 625 to 700 nm. Due to orders of magnitude difference between samples, the integrated values were taken and plotted on a logarithmic scale in Figure 2. (Tabulated raw data can be found in Supporting Information, Table S1.)

In all sample types, an increase in upconversion luminescence is observed in both green and red up to a maximum luminescence occurring at 600 °C in UC1 and 500 °C in UC2 and UC3. Increasing the annealing temperature further results in subsequent decrease in upconversion emission. For all sample types annealed at 700 °C, red emission becomes dominant, with red emission more than an order of magnitude greater than green emission.

All samples were found to be pure β-phase following hydrothermal treatment as confirmed by XRD. The XRD results presented in Figure 3 show a gradual phase change from β to α with full transformation occurring when the sample is annealed at 700 °C. XRD results are similar for all samples

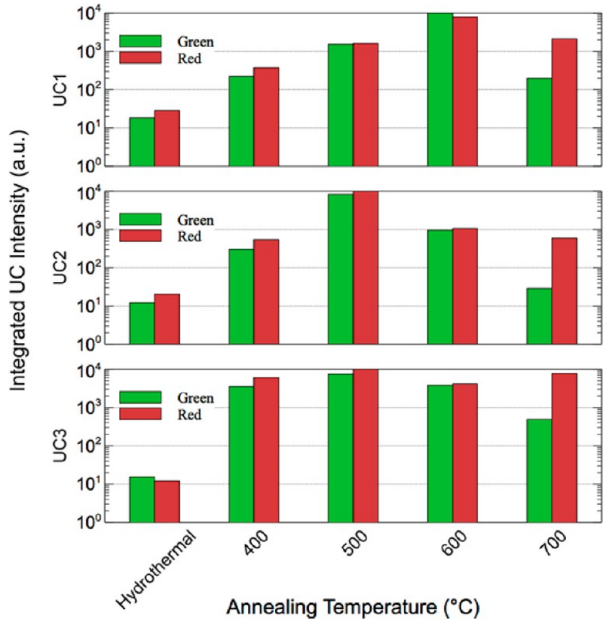

Figure 2. Upconversion emission for samples annealed at different temperatures for UC1 (top), UC2 (middle), and UC3 (bottom). The log is taken for the integrated peak values, and each gridline represents a decade.

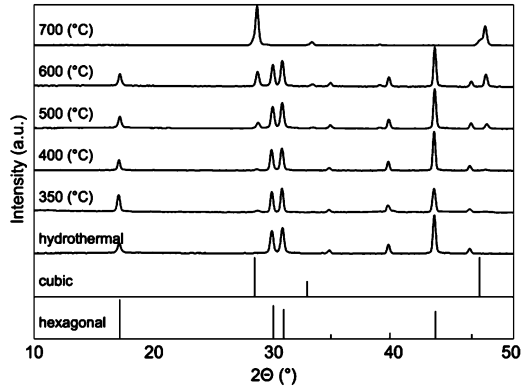

Figure 3. XRD results from UC3 showing gradual phase transformation from β to α via annealing. Reference patterns are shown for cubic (JCPDS 06-0342) and hexagonal (JCPDS 28-1192) phases.

examined in this study and thus only results from the UC3 samples are shown (other samples can be found in the Supporting Information, Figures S4−S6; note the potential formation of YOF in addition to the α-phase, especially at 700 °C, which cannot be ruled out due the close proximity of XRD peaks and the complicating factor of dopant ions in the lattice. This could be the topic of future investigations).

Increasing the temperature increases upconversion luminescence to a point, after which upconversion performance diminishes. This is attributed to the β- to α-phase transition. The NaF-REF_3 phase diagrams are well-known and indicate that this transition temperature should occur at 691 °C, 562 °C, and 702 °C for $NaREF_4$ (RE = Y, Yb, and Er, respectively).[32] As such, it is reasonable to assume the phase transformation will occur within this range of temperatures. According to the XRD results presented in Figure 3, α-phase peaks begin to appear at temperatures as low as 400 °C. With increasing temperature, the strength of the α peaks increase relative to the β peaks with full transformation to α-phase at 700 °C. It is well-

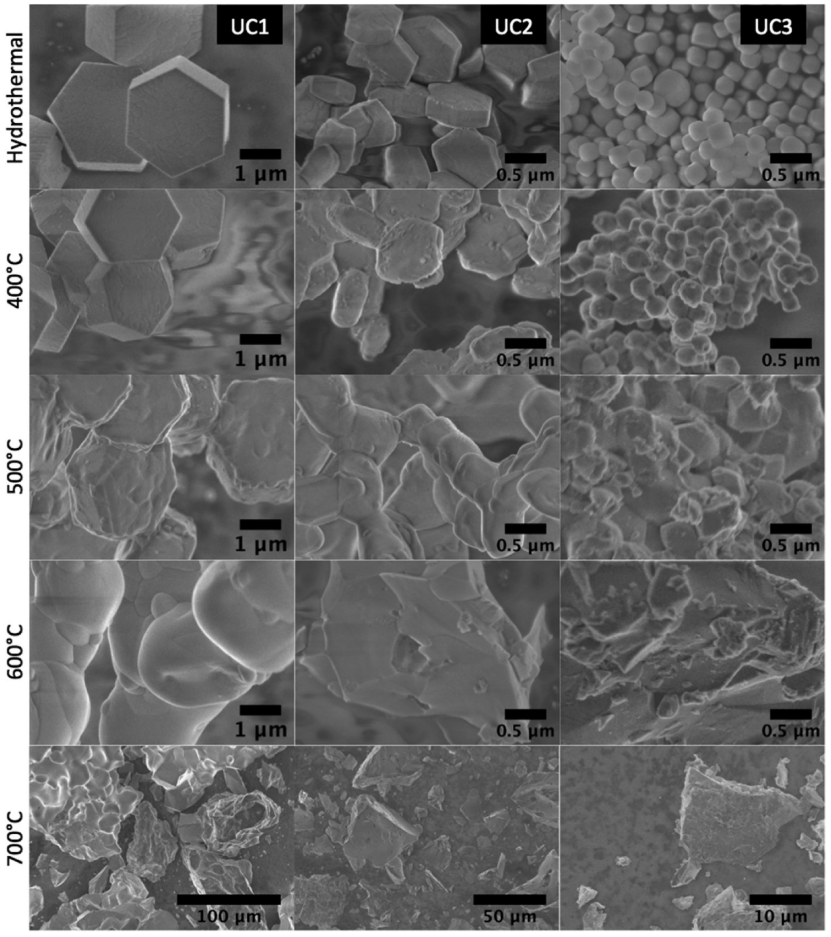

Figure 4. SEM micrographs of different size upconversion crystals showing the effect of annealing temperature on morphology (UC1 left, UC2 middle, UC3 right).

known that the α-phase is a poorer upconverter compared with its β-phase counterpart[3] so as the material transforms, the overall upconversion performance decreases and red emission cannibalizes green. This explains the decreases seen in annealing temperatures higher than the maximal point where the undesirable effects of the β to α phase transition overtake the beneficial effects of the annealing.

To better understand the relationship between crystal morphology and upconversion fluorescence, the particle morphology as a function of annealing temperature was investigated using SEM. The SEM micrographs are presented in Figure 4.

It is clear from the SEM micrographs that crystal morphology was changed significantly because of annealing. As the temperature increases, the surface of the particles begins to roughen and particles begin to agglomerate. An additional UC3 sample annealed at 350 °C was prepared to further investigate the agglomeration onset in the submicrometer sized particles. The TEM morphology for UC3−350 is shown in Figure 5. While some aggregation is observed, sharp interfaces are still observed between the majority of particles and larger agglomerate networks have yet to form. The upconversion luminescence of this sample is slightly lower than UC3−400 but within the same order of magnitude for both green and red emission (see Supporting Information, Table S1) rendering this material of great interest for applications in photonic and photovoltaic devices and in vitro biological applications.

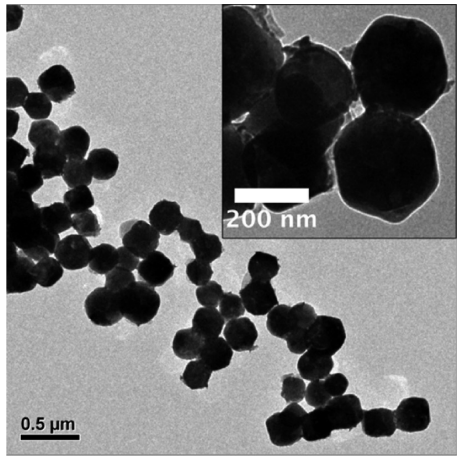

Figure 5. TEM micrograph of UC3 crystals annealed at 350 °C for 2 h.

The morphology changes follow the same general mechanism in all size types, first with roughening of the crystal surfaces (onset at 500 °C for UC1, 400 °C for UC2, and 350 °C for UC3), then agglomeration (onset at 600 °C for UC1, 500 °C for UC2, 400 °C for UC3), and finally formation of bulk sized particles (700 °C for UC1, 600 °C for UC2 and UC3).

The presence of organic molecules can quench the upconversion luminescence as already mentioned. In order to determine the presence of citrate on the surface of the upconversion particles, ATR-FTIR was performed on the hydrothermal (HT) samples and samples annealed at 400 and 500 °C, shown in Figure 6.

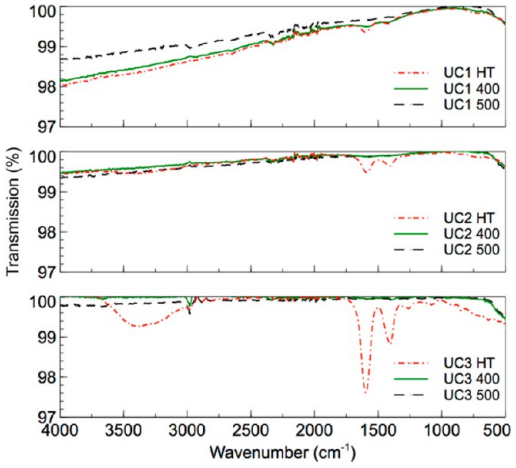

Figure 6. ATR-FTIR transmission spectra of hydrothermally produced upconversion samples including samples annealed at 400 and 500 °C. All spectra were corrected for the ATR effect using the supplied software.

From the FTIR spectra, peaks are observed at ~1430, ~1610, and 3000−3700 cm^{-1} that correspond to O−H bending, C═O stretching, and O−H stretching, respectively,[29] that confirm the presence of organic citrate moieties. The absorption strength of the peaks corresponds with the amount of citrate initially used in hydrothermal synthesis of the different size crystals (Table 1) and the expected increase in surface area available for adsorption in the smaller particles. In the UC1 samples, 500 °C is needed to remove the citrate completely, while in the UC2 and UC3 samples, only 400 °C is needed. The slope present in some of the spectra is due to the scattering effects of the larger particles, which is stronger at shorter wavelengths. Removal of citrate is further evidenced by thermogravimetric analysis (TGA) of sample UC3, presented in Figure S2 of Supporting Information. The plot reveals a decomposition temperature of 372 °C, supporting the data obtained from FTIR.

On the basis of these results, it is very clear that annealing increases upconversion luminescence. This effect is initially attributed to removal of the citrate moieties and residual water, as seen from the FTIR results. The high-energy vibrational states in the organic molecules can serve as recombination centers for the upconverted lanthanide states,[25] so removing them helps increases the upconversion luminescence. It is also possible that annealing helps to reduce internal defects in the crystal lattice. Higher temperatures increase the diffusion coefficient of atoms in the lattice, which helps to decrease the total number of crystal defects that would otherwise serve as recombination centers for the upconverted states.

Another effect that must be taken into account is agglomeration-driven crystal growth. The general progression of particle morphology is presented schematically in Scheme 1. As crystal size decreases in upconversion materials (in particular prior to annealing, refer to Figure 2), the upconversion performance also decreases, which is attributed to an increase in surface state recombination centers as well as hindered migration of the intermediate excited states in Yb^{3+}. Conversely, when particles grow and agglomerate, a similar increase in upconversion luminescence is expected. According to SEM analysis, crystal agglomeration is observed at 600 °C for UC1, 500 °C for UC2, and 400 °C for UC3. Therefore any increases in upconversion prior to agglomeration can be attributed to citrate removal and crystal refinement however the drastic increase at the maximum point for each sample (600 °C in UC1 and 500 °C in UC2 and UC3) is also because of an effective increase in crystal size accompanied by continued crystal refinement.

Crystal morphology is very important to certain technological applications such as dye sensitized solar cells and in vitro biological applications and therefore agglomeration should be avoided.[5,30,33] The maximum upconversion in our samples without particle agglomeration occurs at 500 °C for UC1, 400 °C for UC2, and 350 °C for UC3. It is highly notable that the initial size of the particles impacts the onset of particle roughening and particle agglomeration. The results show that the smaller the particle size, the sooner the onset of roughening and agglomeration. This can be attributed to greater surface area in smaller particles and therefore greater surface area contact between particles and a greater thermodynamic driving force to reduce the surface free energy. Agglomeration occurs first by a roughening of the particle surface, followed by sintering, forming interconnected networks of particles, and finally by growth into larger, bulk sized particles.

While the maximum upconversion comes with a loss of the original particle morphology, a stark increase (orders of magnitude) in upconversion is still observed from the hydrothermal samples to samples just before onset of particle agglomeration, showing that size-dependent controlled annealing can be used to drastically increase upconversion while maintaining the integrity of the original particles. To accurately compare the optical properties of the present upconversion crystal samples with those in literature, the quantum yield of the upconversion process was measured in the hydrothermal samples and the annealed samples before the onset of agglomeration.

Scheme 1. Schematic Illustrating the Changes in Particle Morphology with Increasing Temperature

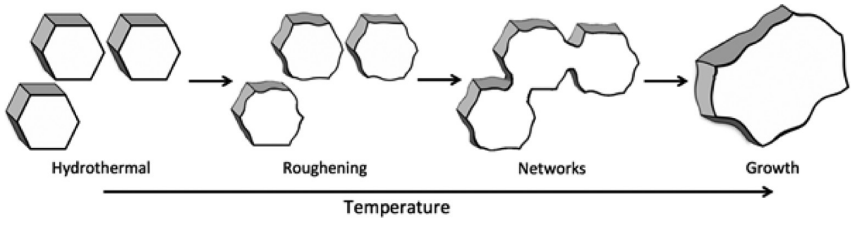

Table 2. Quantum Yields for Hydrothermal Samples and Highest Emitting, Nonagglomerated Annealed Samples

sample	annealing temperature (°C)	power (W/cm^2)	green QY (%)	red QY (%)	total QY (%)	annealing enhancement factor
UC1	N/A	50	0.006 ± 0.01	0.006 ± 0.01	0.01 ± 0.02	
	500	50	1.3 ± 0.3	1.5 ± 0.3	2.7 ± 0.5	270×
UC2	N/A	50	0.01 ± 0.01	0.01 ± 0.01	0.03 ± 0.02	
	400	50	1.8 ± 0.4	3 ± 0.6	4.8 ± 1	160×
UC3	N/A	50	0.02 ± 0.01	0.03 ± 0.01	0.05 ± 0.02	
	350	50	0.9 ± 0.2	1.6 ± 0.3	2.5 ± 0.5	50×

The quantum yield (QY) is calculated using the following equation:[31]

$$\mathrm{QY} = \frac{E_{\mathrm{emission}}}{E_{\mathrm{ref}} - E_{\mathrm{sample}}}$$

Here, E_{emission} is the integrated emission peak (500−575 nm for green or 625−700 nm for red), giving the number of photons emitted, E_{ref} is the integrated laser peak after absorption and scattering from an undoped reference ($NaYF_4$) sample and E_{sample} is the integrated laser peak of the sample itself, with their difference giving the number of photons absorbed. A sample of the upconverted visible and the NIR laser spectra for an individual measurement is provided in Figure S3, Supporting Information. As upconversion to green or red requires 2 absorbed photons for each emitted photon, the quantum yield will therefore range from 0 to 50%. For each sample measured, an undoped reference sample was prepared in the exact same manner, including annealing, to most closely reproduce the scattering of the doped sample. The results from these measurements are presented in Table 2.

The quantum yield of the upconversion process in the hydrothermal samples is relatively low, on the order of about 0.01−0.05% for all samples studied, however when annealing is employed, the quantum yield can be increased by more than 2 orders of magnitude. Notably, the quantum yield of the small sized UC3 particles (~300 nm) can be increased to about 2.5%, an achievement that begins to approach that of the larger particles in the current study and bulk particles (>4 μm) in other studies.[31,34] It should be noted that the power density listed in Table 2 was estimated by measuring the distance from the laser to the center of the integrating sphere and using burn paper to measure the laser spot size and is intended as a rough estimate only.

4. CONCLUSIONS

The size-dependent effect of annealing on phase, morphology, and upconversion luminescence has been investigated systematically by varying the annealing temperature and initial crystal size of $NaYF_4$:Yb^{3+},Er^{3+} upconversion phosphors. It has been found that a gradual phase transition from the β- to the α-phase occurs beginning with annealing temperatures as low as 400 °C, increasing the relative amount of α-phase as temperature increases, and resulting in full transformation to the α-phase at 700 °C regardless of initial particle size. In general, as the temperature is increased, particles first begin to roughen, (350 °C in the 300 nm particles, 400 °C in the 700 nm particles, and 500 °C in the 2.3 μm particles), then form interconnected networks (400 °C in the smallest, 500 °C in the midsized, 600 °C in the largest particles), and finally transform to bulk-sized particles (600 °C in the smallest and midsized particles, 700 °C in the largest). Annealing increases the upconversion luminescence in all samples compared to their hydrothermal counterparts by at least 1 order of magnitude. Prior to particle agglomeration, this increase is attributed to removal of organic surface molecules and crystal refinement through removal of internal defects that otherwise provide recombination pathways for the excited ion states. The upconversion luminescence reaches a maximum when particles initially form networks, which is a result of the effective increase in particle size in addition to the effects already mentioned. Annealing at higher temperatures will cause a subsequent decrease in upconversion luminescence due to conversion to the α-phase, which is a poorer upconverter than the β-phase. In summary, the maximum upconversion luminescence while avoiding particle agglomeration is found at 350 °C for the 300 nm particles, 400 °C in the 700 nm particles and at 500 °C for the 2.3 μm particles. Most notably, the quantum yield can be increased by 2 orders of magnitude in the 300 nm particles to about 2.5% while still maintaining particle shape, approaching the quantum yield of much larger particles measured in other studies. This shows that annealing can be used to maximize the upconversion in nano- to microscale upconversion phosphors while maintaining particle shape and that the annealing profile should be tailored depending on the original particle size and shape.

■ ASSOCIATED CONTENT

Supporting Information

Raw data and additional characterization information and figures. This material is available free of charge via the Internet at http://pubs.acs.org.

■ AUTHOR INFORMATION

Corresponding Author

*E-mail: george.demopoulos@mcgill.ca.

Notes

The authors declare no competing financial interest.

■ ACKNOWLEDGMENTS

This work was funded by NSERC through a strategic project grant to G.P.D. and sponsored by Targray Technology International, Versatilis, CIS Solar, and Hydro-Quebec's IREQ. N.D. is also the recipient of an Alexander Graham Bell CGS Scholarship from NSERC. Quantum yield measurements were completed at the University of Victoria under the direction of Prof. van Veggel and Dr. Jothirmayanantham Pichaandi.

■ REFERENCES

(1) Suyver, J. F.; Aebischer, A.; Biner, D.; Gerner, P.; Grimm, J.; Heer, S.; Krämer, K. W.; Reinhard, C.; Güdel, H. U. *Opt. Mater. (Amsterdam, Neth.)* **2005**, *27*, 1111−1130.

(2) Suyver, J. F.; Grimm, J.; van Veen, M. K.; Biner, D.; Krämer, K. W.; Güdel, H. U. *J. Lumin.* **2006**, *117*, 1−12.

(3) Kramer, K.; Biner, D.; Frei, G.; Gudel, H. *Chem. Mater.* **2004**, *16*, 1244−1251.

(4) Van De Rijke, F.; Zijlmans, H.; Li, S.; Vail, T.; Raap, a K.; Niedbala, R. S.; Tanke, H. J. *Nat. Biotechnol.* **2001**, *19*, 273−276.
(5) Yi, G.; Lu, H.; Zhao, S.; Ge, Y.; Yang, W.; Chen, D.; Guo, L.-H. *Nano Lett.* **2004**, *4*, 2191−2196.
(6) Chen, Z.; Zhang, L.; Sun, Y.; Hu, J.; Wang, D. *Adv. Funct. Mater.* **2009**, *19*, 3815−3820.
(7) Yu, X.; Li, M.; Xie, M.; Chen, L.; Li, Y.; Wang, Q. *Nano Res.* **2010**, *3*, 51−60.
(8) Downing, E.; Hesselink, L.; Ralston, J.; Macfarlane, R. *Science* **1996**, *273*, 1185−1189.
(9) Zhang, F. F.; Wan, Y.; Yu, T.; Shi, Y.; Xie, S.; Li, Y.; Xu, L.; Tu, B.; Zhao, D. *Angew. Chem.* **2007**, *119*, 8122−8125.
(10) McFarlane, R. A. *Opt. Lett.* **1991**, *16*, 1397−1399.
(11) Shalav, A.; Richards, B. S.; Green, M. A. *Sol. Energy Mater. Sol. Cells* **2007**, *91*, 829−842.
(12) De Wild, J.; Meijerink, A.; Rath, J. K.; van Sark, W. G. J. H. M.; Schropp, R. E. I. *Energy Environ. Sci.* **2011**, *4*, 4835−4848.
(13) Cheng, Y. Y.; Fückel, B.; MacQueen, R. W.; Khoury, T.; Clady, R. G. C. R.; Schulze, T. F.; Ekins-Daukes, N. J.; Crossley, M. J.; Stannowski, B.; Lips, K.; Schmidt, T. W. *Energy Environ. Sci.* **2012**, *5*, 6953−6959.
(14) Li, C.; Yang, J.; Yang, P. *Cryst. Growth Des.* **2008**, *8*, 923−929.
(15) Zhang, F.; Li, J.; Shan, J. *Chem.—Eur. J.* **2009**, *15*, 11010−11019.
(16) Zhou, J.; Chen, G.; Wu, E.; Bi, G.; Wu, B.; Teng, Y. *Nano Lett.* **2013**, *13*, 2241−2246.
(17) Yuan, D.; Tan, M. C.; Riman, R. E.; Chow, G.-M. *J. Phys. Chem. C* **2013**, *117*, 13297−13304.
(18) Sun, Y.; Chen, Y.; Tian, L.; Yu, Y.; Kong, X.; Zhao, J.; Zhang, H. *Nanotechnology* **2007**, *18*, 275609.
(19) Wang, F.; Han, Y.; Lim, C. S.; Lu, Y.; Wang, J.; Xu, J.; Chen, H.; Zhang, C.; Hong, M.; Liu, X. *Nature* **2010**, *463*, 1061−1065.
(20) Auzel, F. *Chem. Rev.* **2004**, *104*, 139−173.
(21) Dong, C.; Pichaandi, J.; Regier, T.; van Veggel, F. C. J. M. *J. Phys. Chem. C* **2011**, *115*, 15950−15958.
(22) Yuan, D.; Shun, Yi, G.; Chow, G. M. *J. Mater. Res.* **2009**, *24*, 2042−2050.
(23) Xue, X.; Uechi, S.; Tiwari, R. N.; Duan, Z.; Liao, M.; Yoshimura, M.; Suzuki, T.; Ohishi, Y. *Opt. Mater. Express* **2013**, *3*, 989−999.
(24) Wu, S.; Ning, Y.; Chang, J.; Zhang, S. *J. Lumin.* **2013**, *143*, 492−497.
(25) Wang, Y.; Tu, L.; Zhao, J.; Sun, Y. *J. Phys. Chem. C* **2009**, *113*, 7164−7169.
(26) Mai, H.; Zhang, Y. *J. Phys. Chem. C* **2007**, *111*, 13721−13729.
(27) Yi, G.; Chow, G. *Chem. Mater.* **2007**, *19*, 341−343.
(28) Fu, J.; Fu, X.; Wang, C.; Yang, X.; Zhuang, J.; Zhang, G.; Lai, B.; Wu, M.; Wang, J. *Eur. J. Inorg. Chem.* **2013**, *2013*, 1269−1274.
(29) Assaaoudi, H.; Shan, G.-B.; Dyck, N.; Demopoulos, G. P. *CrystEngComm* **2013**, *15*, 4739−4746.
(30) Shan, G.-B.; Assaaoudi, H.; Demopoulos, G. P. *ACS Appl. Mater. Interfaces* **2011**, *3*, 3239−3243.
(31) Boyer, J.-C.; van Veggel, F. C. J. M. *Nanoscale* **2010**, *2*, 1417−1419.
(32) Thoma, R.; Insley, H.; Hebert, G. *Inorg. Chem.* **1966**, *1005*, 1222−1229.
(33) Han, C.; Lee, H.; Lee, K. *Bull. Korean Chem. Soc.* **2009**, *30*, 219−223.
(34) Faulkner, D. O.; Petrov, S.; Perovic, D. D.; Kherani, N. P.; Ozin, G. A. *J. Mater. Chem.* **2012**, *22*, 24330−24334.